periodica polytechnica

Civil Engineering
56/1 (2012) 87–95
doi: 10.3311/pp.ci.2012-1.10
web: http://www.pp.bme.hu/ci

RESEARCH ARTICLE

Identifying wave and turbulence components in wind-driven shallow basins

Krisztián Homoródi / *János* Józsa / *Tamás* Krámer / *Giuseppe* Ciraolo / *Carmelo* Nasello

Received 2011-05-02, revised 2011-06-02, accepted 2011-10-12

Abstract

Wind-induced waves play an important role in shallow lake hydro- and sediment dynamics. That is why field measurements are important for the validation of their estimation methods, especially in shallow waters. In the first part of the present paper a method is introduced to improve the interpretation of the measured data, applicable both for pressure and velocity data. Replacing the turbulence-affected tail of the measured spectrum with a fitted power function causes a considerable 8-10% difference in the derived bulk wave parameters so this procedure is worth to be done. In the second part an appropriate technique to obtain wave features from 3D velocity time series will be described. The applicability of the presented velocity-based estimation method will be proved by the analysis of field measurements. By velocity decomposition used for the reconstruction of wave features one could also analyse the depth-related differences in the turbulence accompanying the wave motion.

Keywords

wave measurement · shallow lake · lagoon · velocity decomposition · wave motion · turbulence

Acknowledgement

This work is connected to the scientific program of the "Development of quality-oriented and harmonized R+D+I strategy and functional model at BME" project, supported by the New Széchenyi Plan (Project ID: TÁMOP-4.2.1/B-09/1/KMR-2010-0002).

Krisztián Homoródi
János Józsa
Tamás Krámer

Budapest University of Technology and Economics, Department of Hydraulic and Water Resources Engineering, H-1111 Budapest, Műegyetem rakpart 3. Kmf. 12, Hungary

Giuseppe Ciraolo
Carmelo Nasello

University of Palermo Department of Civil, Environmental and Aerospace Engineering, I-90128 Palermo, Viale delle Scienze – Ed. 8, Italy

1 Introduction

Wind-induced waves are known to play an important role in shallow lakes hydro- and sediment dynamics, e.g. in bed material stirring-up or wave loading on beach protection works. Field measurements and their analysis are still essential to obtain a better, more detailed insight to wave features in shallow conditions. Data are also important for the validation of various wave estimation formulas or numerical models in the given application conditions, similarly to the setup of hydrodynamic models for lakes (see e.g. Krámer and Józsa, 2005) or rivers (see e.g. Baranya and Józsa, 2006).

In the first part of the present paper a method is introduced to improve the processing of the measured data, applicable both for pressure and velocity time series. In fact, pressure-based wave measurement has a deficiency because it is not able to provide information about the direction of the waves, though in addition to the wave height, direction is another relevant parameter in e.g. beach protection or harbour planning. Using several synchronised gauges it is possible to derive some kind of directional data but this is far from being a general solution. In turn, 3D velocity measurement data inherently contain directional information. In the second part of the paper an appropriate technique to obtain wave features from 3D velocity time series, in general containing also seiche, circulatory and turbulent components is demonstrated. This method was validated by pressure-based data and analysis of synchronised velocity measurements at different depths in a vertical. By velocity decomposition one could also analyse the depth-related differences in the wave motion parameters and the turbulence accompanying the wave motion.

2 Measurement location and tools

Recently two shallow water bodies, Lake Neusiedl at the Austro-Hungarian border and the Stagnone di Marsala lagoon in Sicily have been studied to this aim (Fig. 1). Besides wave measurements there were also 2D velocity measurements in Lake Neusiedl which were used for calibration of a 2D hydrodynamic model of the lake (Krámer and Józsa, 2005).

A unique feature of Lake Neusiedl is its huge littoral reed belt

(indicated in gray), with large reed patches also in the pelagic area. Though the water exchange, siltation and wave attenuation processes are very important in the reed zones, the first investigations focused on the pelagic areas, simpler for deploying the measurement device. In the lake three wave measurement campaigns were conducted. In the first and the second campaigns a standard wave pressure gauge was used. It was placed directly on the lake bottom. The depth of lake was as small as 1.0-1.1 m thus the sensor head was 0.60 m below the mean water surface. Wave data were collected using 5-min bursts with 8 Hz sampling rate, triggered every 30 min. In the third campaign 3D velocities were measured in two points by 2 Nortek Vectrino current meters at 25 Hz sampling rate, at 0.4 and 1.2 m under water surface, in a total depth of 1.6 m. The sensors were oriented so as to minimise the perturbation of the measurements in the predicted average direction of wave propagation. Beside water pressure and velocity, wind speed and direction were also measured at the same location at 3.3-3.5 m height above the surface at 1/30 Hz sampling rate. The measurement location was chosen to provide more than 10-km fetches for the prevailing N-NW wind directions.

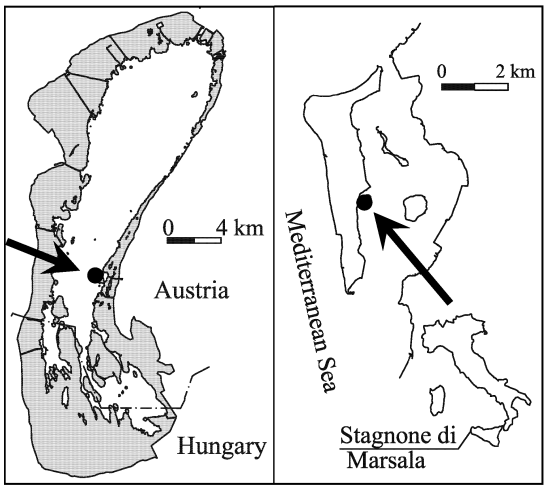

Fig. 1. Measurement locations in Lake Neusiedl (left) and Stagnone di Marsala (right)

As to the lagoon of Stagnone di Marsala, its depth and fetches are similar to those of Lake Neusiedl, except for its salinity and vegetation, certainly affecting the wave properties. There pressure, 3D velocities were measured by a Nortek Vector ADV at 16 Hz sampling rate, continuously in about hour-long intervals. The pressure and the velocity sensors were at 0.23 and 0.60 m below the mean surface, respectively, in a total depth of 1.25 m. Wind speed and direction were also measured at the same location at 3.0 m height above the surface (Fig. 2) at 1/60 Hz sampling rate.

3 Analysis of pressure measurements

As was mentioned above, at both water bodies surface wave motion was reconstructed from pressure time series. However, in such a case a compensation procedure has to be applied due

Fig. 2. The platform of the current and wind measurements on the Stagnone di Marsala

to the exponential attenuation of wave-induced pressure fluctuations with depth. The higher the frequency, the larger the attenuation. To keep this compensation in a manageable range the sensor should be deployed as close to the surface as possible, though strictly below the lowest expected water level in a combined seiche and wave motion. These criteria were reasonably met in our campaigns.

As attenuation depends on wave frequency, the compensation has to be carried out by spectral decomposition instead of time domain analysis. A standard procedure for that is the computation of the spectrum of the pressure $Z_p(f)$ using discrete Fourier transformation (DFT), from which the spectrum of surface elevation $Z(f)$ is then obtained by scaling $Z_p(f)$ with the assumption of linear wave theory and zero phase shift (see e.g. Massel, 1996) as follows:

$$Z(f) = \frac{Z_p(f)}{g\rho_w} \cdot \frac{\cosh\left[k(f)h\right]}{\cosh\left[k(f)(h-h_p)\right]}, \qquad (1)$$

with g = acceleration due to gravity; ρ_w= water density; h = total water depth measured from the mean water level; h_p = depth of the pressure sensor; $k(f)$ = wave number of the harmonic wave component with frequency f, defined implicitly by the dispersion relation, $(2\pi f)^2 = gk \tanh kh$. The first fraction on the right is the hydrostatic pressure head and the second fraction reverses depth-attenuation by a frequency-dependent amplitude modulation. The compensation is done for 5-min windows at a time (coincidentally the length of one burst of the wave gauge).

Due to this attenuation the high frequency range of the spectrum is not likely to be related to the wave motion, instead, it is expected to represent the energy in turbulence, along with some possible measurement noise. That is why the wave-related compensation is not applicable here, as can be seen on the unrealistically excessive amplification in the high-frequency range in Fig. 3. To avoid this, an upper threshold for the frequencies to be compensated has to be chosen. Note that on Fig. 3 and subsequently we plot the energy per unit weight, $E(f) = |Z(f)|^2$.

Wave components beyond the threshold frequency still play

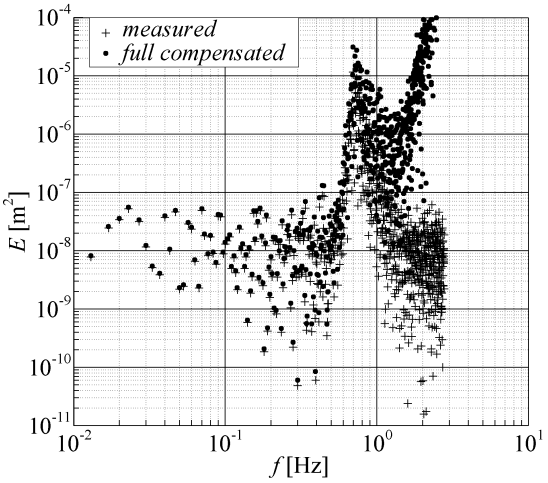

Fig. 3. Original energy spectrum of a typical 5-min burst (crosses) and its compensation over the full frequency range (dots).

a role in determining the bulk wave parameters (e.g. average wave height and period) but are absent in the original spectrum. To cure that, the turbulence-dominated tail of the spectrum is replaced by a fitted analytical power function (Fig. 4) based on the Pierson-Moskowitz or the JONSWAP spectrum (WMO, 1998), both characterised by an f^{-b} power law, where $b = -5$.

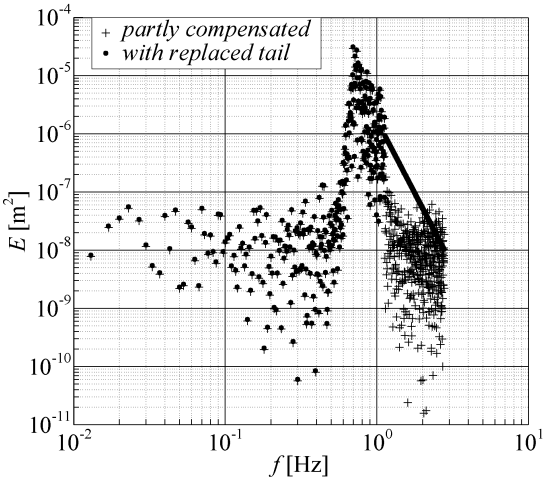

Fig. 4. Energy spectrum in Fig. 3 compensated partly (i.e. for lower frequencies) with (dots) and without the replaced tail (crosses).

It is to be noted that Prevosto et al. (1996) found the exponent -4 in deep water, whereas Rodríguez and Soares (1999) found it to fall between -4 and -6. When investigating the great number of bursts from Lake Neusiedl, we found the best fitting exponent varying as seen in Fig. 5, with -4 as most frequent and -5 as average integer value, though rather flat in the $(-3, -5)$ interval.

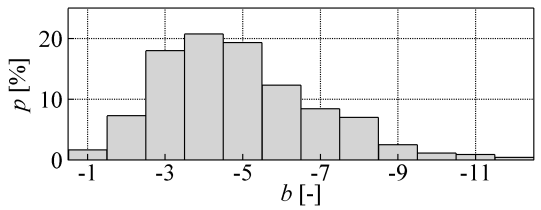

Fig. 5. A histogram of the exponent b of the fitted tail.

Based on this we accepted –5 for further calculations. The spectrum should be lengthened until four times the peak frequency (Prevosto et al. 1996; Rodríguez and Soares 1999). The difference between partly compensated spectra and the spectra with replaced tail has been quantified via bulk wave parameters such as the spectral wave height (H_{m0}) and period (T_{m01}). We found that the average relative differences were $\Delta H_{m0} = +8\%$ and $\Delta T_{m01} = -12\%$, respectively. These differences justify the application of the outlined procedure.

4 Analysis of velocity measurements

In the following the method and the results of the analysis of velocity measurements are described. The method was the same at both campaigns. At first it is described with the results of the measurements on Lake Neusiedl, and then the results of the measurements on Stagnone di Marsala lagoon are shown.

4.1 Velocity measurements on Lake Neusiedl

Beside wave related and turbulence components the measured velocity time series also contain larger timescale components such as circulatory currents and seiche that need to be subtracted before further analysis.

Fig. 6 shows a shorter portion of a characteristic 5-min window of the velocity measurements. The method of analysis will be illustrated with this window throughout this section.

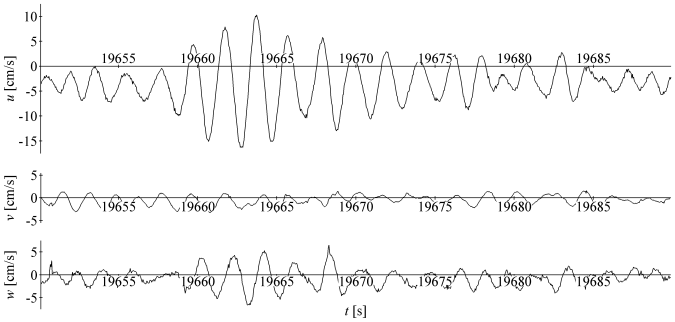

Fig. 6. 30 seconds of simultaneous time series of the measured velocity components (u North, v East and w upward directions).

The long wave components such as circulatory currents and seiche were removed using standard Kaiser window based high pass filtering with a cutoff frequency of 1/3 Hz, which bounds the expected range of wind waves from below. This cutoff frequency was found to apply uniformly throughout the measurement period as is also confirmed in the energy spectrum of the selected 5-min window (Fig. 7).

Comparing these slowly varying components in the two different depths with each other, furthermore, with the wind speed vector (Fig. 8) the whole measurement period can be separated into two characteristic parts. At wind speeds lower than 4 m/s, in the first 3/4 of the time a flow going with the wind near the surface is accompanied with reverse flow near the bed, providing a velocity profile typical to deep conditions (deep relative to the significant surface wave length). In turn, a wind speed exceeding 6 m/s in the rest of the time resulted in a clear unidirectional,

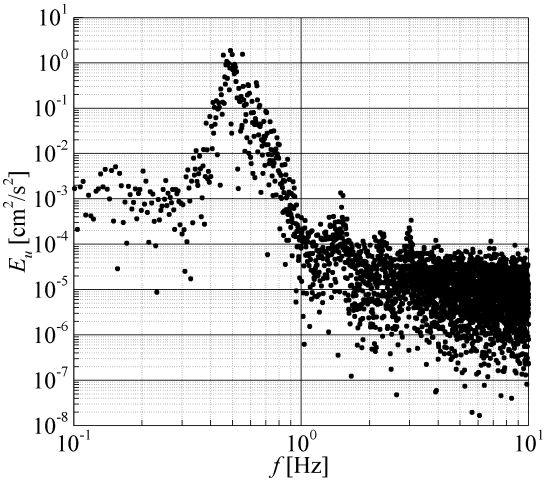

Fig. 7. Energy spectrum of the u (North) component of the measured velocity time series for the 5-min window.

strongly wind-oriented flow profile that extended uniformly to most of the depth in the period of the strongest winds.

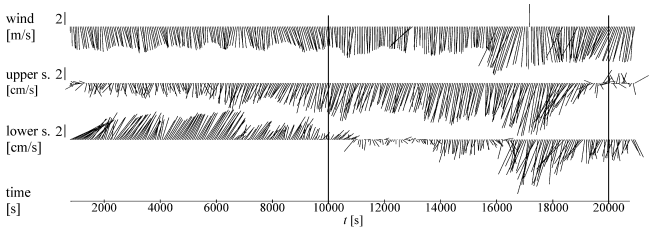

Fig. 8. Low pass filtered wind speed (top) and simultaneous horizontal flow velocity vector time series at the upper and lower sensor resampled at 1-min interval.

Finally, the applied high pass filtering provided time series that contain wave and turbulence components only. When a monochromatic wave is investigated, based on the linear wave theory the following equation holds between the surface displacement and the horizontal component of the velocity (see e.g. Dean & Dalrymple, 1984):

$$\eta(x,t) = \frac{H}{2}\cos(kx-\omega t) = \frac{u(x,z,t)}{\omega}\cdot\frac{\sinh(kh)}{\cosh[k(h+z)]}, \tag{2}$$

where $\eta(x,t)$ = surface displacement with mean horizontal position x and time t; H = wave height; ω = circular frequency; $u(x,z,t)$ horizontal velocity component at x horizontal, z mean vertical position and t time. For the vertical component of the velocity we obtain

$$\frac{H}{2}\sin(kx-\omega t) = \frac{w(x,z,t)}{\omega}\cdot\frac{\sinh(kh)}{\sinh[k(h+z)]}, \tag{3}$$

that is, the second equation yields the time series of surface displacement but with 90° phase shift.

In fact, like for the pressure, the attenuation of the velocity depends on the wave frequency. That is why its required compensation is carried out in the spectral domain:

$$Z(f) = \frac{Z_u(f)}{\omega}\cdot\frac{\sinh(kh)}{\cosh[k(h+z)]}, \tag{4}$$

$$Z(f) = \frac{Z_w(f)}{\omega}\cdot\frac{\sinh(kh)}{\sinh[k(h+z)]}, \tag{5}$$

However, this technique can be applied only on the orbital velocity components, while the measured velocity time series also contain mean current, lake-wide seiche and turbulence components (as was seen in Fig. 6). Therefore these longer and shorter components must be removed prior to the wave analysis. As it was described above the longer components were already removed using high pass filtering. The removal of turbulence needs a more sophisticated approach, as will be described next.

The separation of wave and turbulence related components starts from the energy spectrum of the high pass filtered velocity time series (Fig. 9).

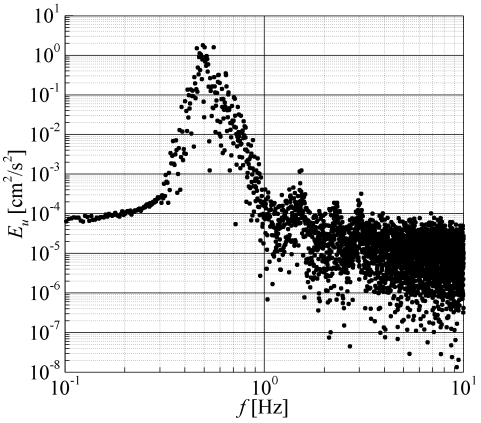

Fig. 9. Energy spectrum of the high pass filtered velocity time series for the 5-min window (u, Noth component).

As can be seen in the figure a clear peak appears due obviously to the high energy content of the dominant wave component, while energy is related mainly to turbulence elsewhere. Following Bricker and Monismith (2007) the turbulence-related spectrum was estimated by cutting off the wave dominated range and replacing it by an extrapolated power function fitted to the remaining parts of the spectrum (Fig. 10). This procedure admits turbulence also in the wave-dominated frequency range, though having minor contribution to the energy.

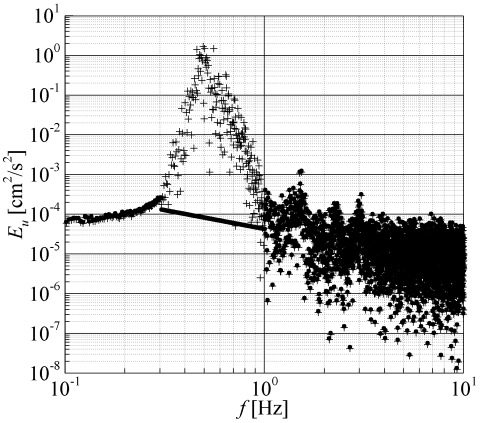

Fig. 10. The energy spectrum of the high pass filtered velocity (crosses) and the estimated turbulence energy spectrum (dots) for the 5-min window.

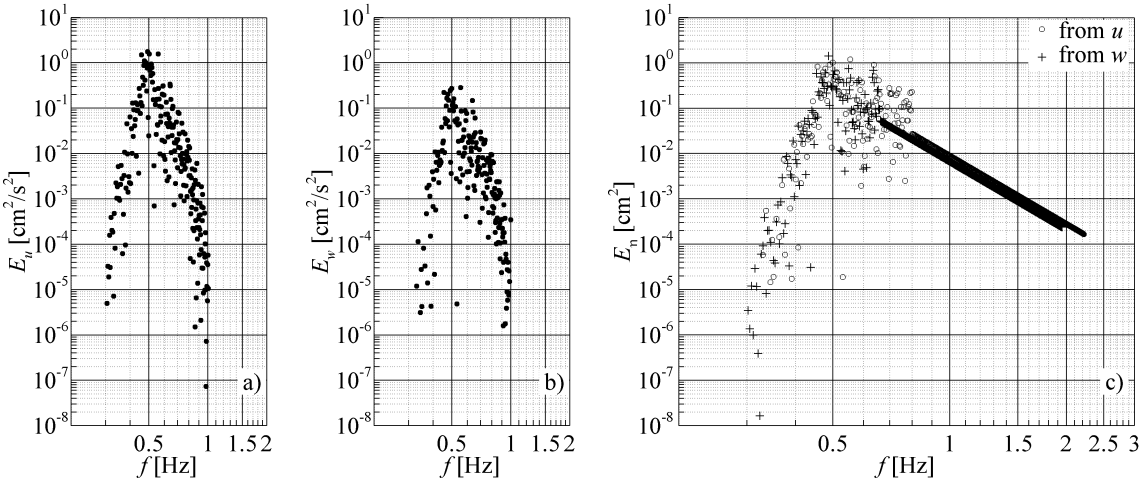

Fig. 13. Energy spectra of horizontal (a) and vertical orbital velocity components (b); and the derived wave energy spectra (c) for the 5-min window.

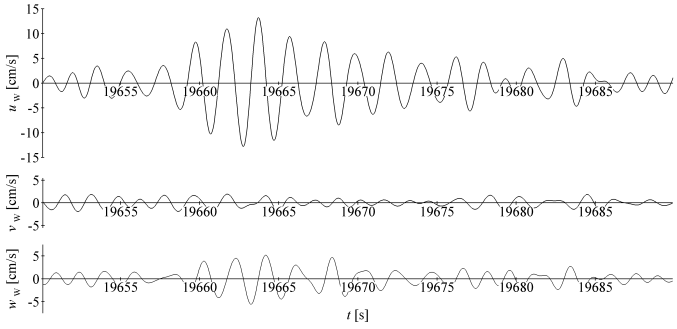

Fig. 11. Simultaneous time series of the orbital velocity components (u North, v East and w upward directions) for the same period as in Fig. 6.

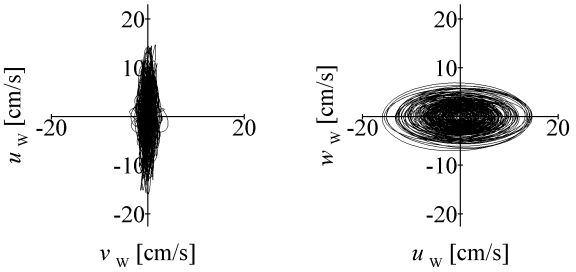

Fig. 12. Excursion of the orbital velocity components in the horizontal and in the wave-aligned vertical plane (u North, v East and w upward directions).

The spectrum of the wave-related orbital velocity components was then readily obtained by subtracting the estimated turbulence spectrum from spectrum of the high pass filtered time series. Finally we obtained the time series of the orbital velocity component by inverse DFT, adopting original phase angles (Fig. 11).

To reconstruct the surface displacement time series from the horizontal component of the orbital velocity only, it is necessary to find the direction of the waves. Of course, the estimation of the wave direction can be also an important issue in itself. In our study the so-called principal component analysis was used to calculate wave direction. This horizontal direction will determine the vertical plane in which the orbital motion occurs. This step is of great importance when processing only horizontal velocity components, because the components in the plane of the orbital motion are required for the direct reconstruction of the surface displacement. The direction of this vertical plane is N-S in this case, thus no co-ordinate transformation was necessary (Fig. 12).

The wave spectrum can be calculated both from the spectrum of the horizontal and the vertical orbital velocity components (Fig. 13 a and b) by using Eq. (4) and Eq. (5), respectively. However, recalling Fig. 10 we can see that the method we applied could not separate turbulence perfectly. In a first trial on compensating the attenuations, the remaining turbulence was indicated by exaggerated amplifications in the high frequency range, similar to the ones observed in the pressure-based analysis, and was treated by appropriately replacing the tail (Fig. 13 c) as developed there.

Using inverse DFT the surface displacement time series were reconstructed separately from the horizontal and vertical components at both measurement depths (Fig. 14). Note the phase shift between the vertical orbital velocity component and the surface displacement, as an expected feature already mentioned when discussing their relationship. The bulk wave parameters can be then calculated from the spectrum, but can also be estimated from the surface displacement time series applying e.g. the zero-downcrossing technique ($\overline{H}$- average wave height, $H_{1/3}$ - significant wave height, $\overline{T}$- average wave period).

To check the validity of the reconstruction procedure in the conditions of Lake Neusiedl, we compared the wave spectra (Fig. 13 c), the surface displacement time series (Fig. 15) and the bulk wave parameters derived from the vertical and the horizontal orbital velocity components as well as the data measured at the two different depths.

Tab. 1 shows some of the calculated wave parameters, as well as their difference for three investigated 5-min windows of the measurement in the Lake Neusiedl. The first window from 14:34 to 14:40 (8366-8697 s from the start of the measurements) was chosen to be representative for the lower wind speed conditions, the second from 16:54 to 17:00 (16732-17078 s) is just after the steep increase of the wind speed, the third from 17:39

to 17:45 (19439-19821 s) was chosen to be representative for the higher wind speed conditions. As is seen, the differences are small enough to prove the consistency of the presented velocity-based estimation method.

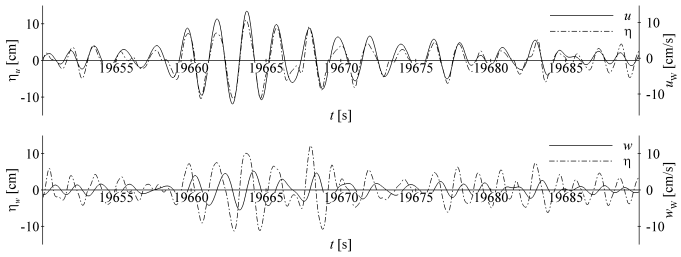

Fig. 14. Time series of the horizontal (upper plot) and vertical (lower plot) orbital velocity components (solid lines) and the reconstructed surface displacement (dashed lines) for the same period as in Fig. 6.

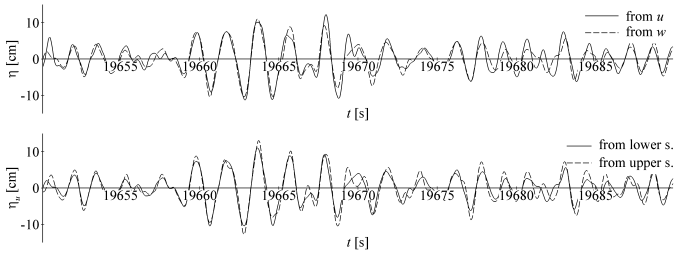

Fig. 15. Reconstructed surface displacement time series, derived from the u and w orbital velocity components at the lower sensor (upper plot), and from the w component at both sensors (lower plot) for the same period as in Fig. 6.

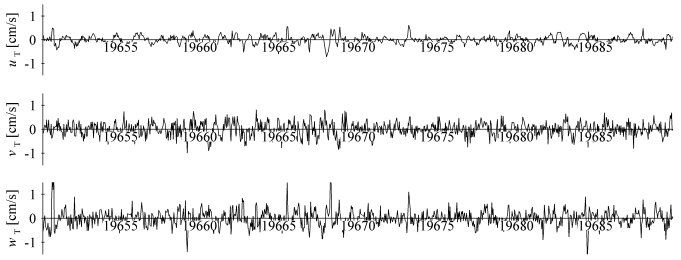

Fig. 16. Time series of the turbulent velocity components for the same period as in Fig. 6: u wave-aligned (North), v transverse (East) and w upward directions.

Removing the orbital velocity component, from the high pass filtered time series the residual is meant to represent turbulence (Fig. 16, Fig. 17). In fact, the auto-correlation functions of this residual time series show a shape typical to conventional turbulence (Fig. 18).

To characterise the turbulence, the kinetic energy and Eulerian timescale were calculated for the three investigated measurement intervals at both depths (Tab. 2). Values show rather low turbulence energy level and the presence of short time period energetic turbulent eddies. As to the total turbulent kinetic energy, it increases significantly at the time of the steep increase in the wind speed, and seemingly remains intensive during the rest of the time, first of all in the upper part of the depth. Note that the Eulerian timescale is rather isotropic in the vertical plane

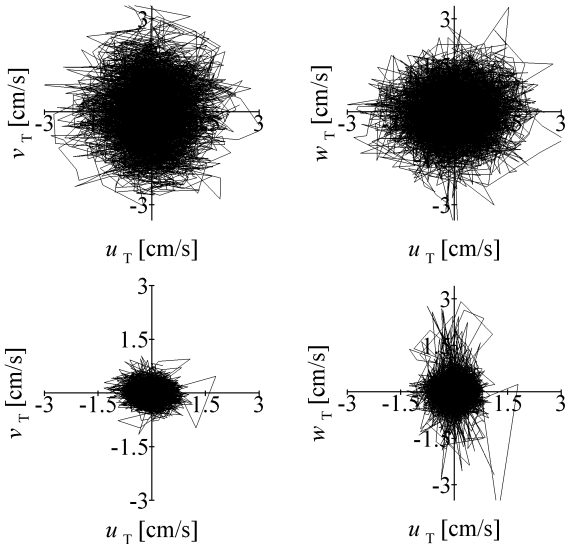

Fig. 17. Excursion of the turbulent velocity components near the surface and the bed during the 5-min window: u wave-aligned (North), v transverse (East) and w upward directions.

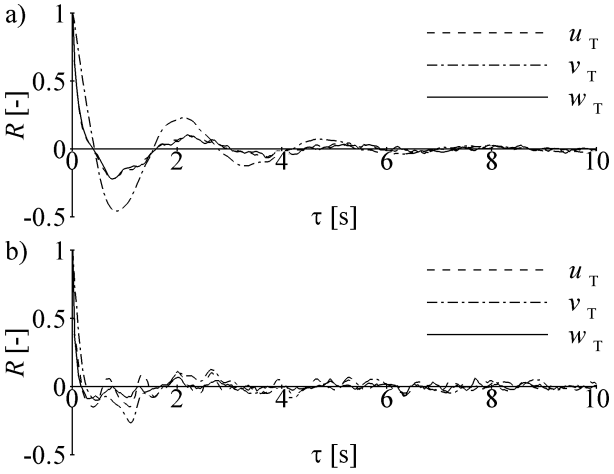

Fig. 18. Auto-correlation function of the turbulence components near the surface (a) and the bed (b).

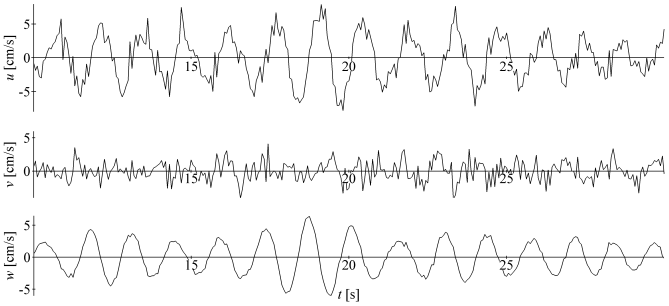

Fig. 19. 20 seconds of simultaneous time series of the measured velocity components (u wave-aligned, v transverse and w upward directions).

of the wave motion (u and w components) whereas systematically different in the direction perpendicular to it, showing anisotropy.

4.2 Velocity measurements on Stagnone di Marsala

The same method of analysis is also applied to the velocity measurements on the Stagnone di Marsala lagoon (Fig. 19).

Tab. 1. Wave height and period derived from horizontal (u) and vertical (w) orbital velocity components and their difference.

		14:34 – 14:40			16:54 –17:00			17:39 – 17:45		
		lower s.	upper s.	Δ	lower s.	upper s.	Δ	lower s.	upper s.	Δ
H_{m0} [cm]	u	6.0	7.9	–1.9	15.9	16.4	–0.5	18.1	19.4	–1.3
	w	6.4	8.6	–2.2	15.8	17.8	–2.0	19.1	20.5	–1.4
	Δ	+0.4	+0.7		–0.1	+1.4		+1.0	+1.1	
T_{m01}[s]	u	1.37	1.23	+0.14	1.49	1.44	+0.05	1.73	1.64	+0.09
	w	1.33	1.14	+0.19	1.47	1.36	+0.11	1.65	1.59	+0.06
	Δ	–0.04	–0.09		–0.02	–0.08		–0.08	–0.05	

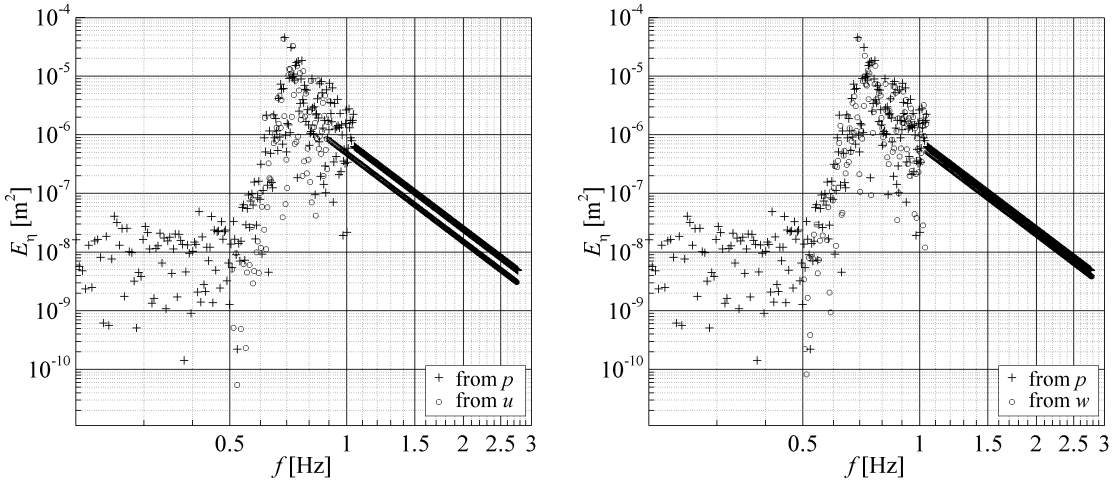

Fig. 20. Wave energy spectra determined from the pressure (crosses on both plots), from the horizontal orbital velocity component (dots on the left plot) and from the vertical orbital velocity component (dots on the right plot).

Tab. 2. Characteristics of the turbulence component (TKE - turbulent kinetic energy, T_E - Eulerian time scale; u wave-aligned (North), v transverse (East) and w upward directions)

		14:34 – 14:40		16:54 –17:00		17:39 – 17:45	
		lower s.	upper s.	lower s.	upper s.	lower s.	upper s.
TKE[cm^2/s^2]	u	0.047	0.048	0.174	0.209	0.048	0.244
	v	0.012	0.015	0.189	0.414	0.019	0.432
	w	0.074	0.048	0.144	0.144	0.067	0.228
	total	0.133	0.110	0.507	0.767	0.134	0.904
T_E[s]	u	0.064	0.053	0.096	0.107	0.076	0.121
	v	0.090	0.100	0.149	0.207	0.126	0.228
	w	0.058	0.056	0.093	0.075	0.068	0.124

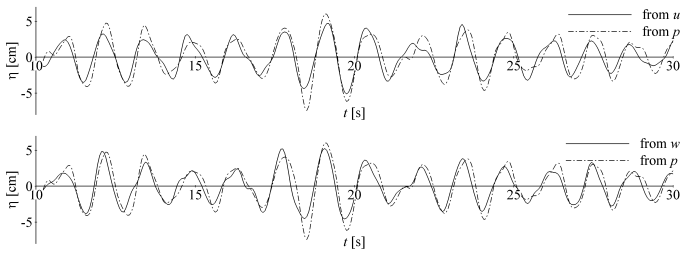

Fig. 21. Surface displacement time series derived from orbital velocity components (solid lines) and from pressure data (dashed lines, same in both panels) for the same period as in Fig. 19.

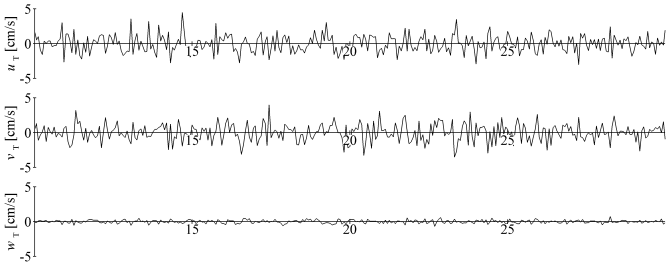

Fig. 22. Time series of the turbulent velocity components for the same period as in Fig. 19: u wave-aligned, v transverse and w upward directions.

Here pressure measurements were used for validation.

The wave spectra (Fig. 20), the surface displacement time series (Fig. 21) and the bulk wave parameters derived both from velocity and pressure measurements were compared. Tab. 3 shows some of the calculated wave parameters, as well as their difference. As is seen, the differences are small enough to prove the applicability of the presented velocity-based estimation method.

Removing the orbital velocity component, from the high pass filtered time series the residual is meant to represent turbulence

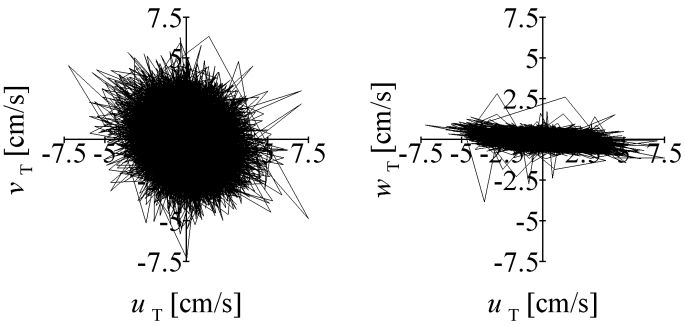

Fig. 23. Excursion of the turbulent velocity components in the horizontal and vertical plane during a 5-min window: u wave-aligned, v transverse and w upward directions.

(Fig. 22, Fig. 23).

To characterise the turbulence, the kinetic energy was calculated (Tab. 4). Velocity was measured at half depth (0.60 m below the mean surface, in a total depth of 1.25 m). The wave conditions during this measurement were close to the first investigated part of the time series measured in Lake Neusiedl so we can compare the turbulence properties of these two intervals.

Tab. 3. Wave parameters derived from orbital velocity components and their difference from pressure data.

	H_{m0} [cm]	ΔH_{m0} [cm]	T_{m01} [s]	ΔT_{m01} [s]
u	7.0	–1.7	1.26	+0.06
w	7.7	–1.0	1.20	–0.01
p	8.7	-	1.21	-

Tab. 4. Turbulent kinetic energy (TKE) values during a characteristic 5-min window for the three orthogonal directions and in total.

	TKE [cm^2/s^2]
u	0.721
v	0.688
w	0.031
total	1.441

In Stagnone di Marsala the turbulent kinetic energy is much higher than in Lake Neusiedl. This higher turbulence can be caused by the irregular seagrass cover of the bottom. In Lake Neusiedl, in contrary, the bed surface is smooth, there is no submerged bottom vegetation, except the reed zone as emergent macrophyte. As to the seagrass in the lagoon, its height is not homogeneous, the higher ones forming a ring-type pattern, a source for generating high turbulence energy level. The turbulent kinetic energy proves to be isotropic in the horizontal plane (u and v components) and anisotropic in the vertical direction. As to the latter, a possible explanation can be that though the measurement point was 0.60 m above the bottom, it was only 0.10-0.20 m above the local seagrass canopy, which damped vertical motions.

5 Conclusion

As was demonstrated in the first part of this paper, replacing the turbulence-affected tail of the measured spectrum with a fitted power function improves bulk wave parameter estimates by a considerable 8 to 10%.

We also described an appropriate technique to obtain wave and turbulence features from 3D velocity time series. As was seen it makes little difference whether we reconstruct the surface displacement from the pressure or the velocity data, so the presented velocity-based estimation method is applicable to shallow lake conditions.

Making use of 3D velocity time series measured at multiple depths in developed wavy conditions in the shallow Lake Neusiedl we could confirm the applicability of wave reconstruction methods conceived earlier.

It is to be noted that when the horizontal velocity is used for the reconstruction, one must take the wave-aligned component. As a consequence this method requires a directional spectrum in case of multidirectional wave conditions. In contrast, the vertical velocity component can be used to reconstruct the surface displacement regardless of wave directionality.

By using suitable velocity decomposition technique we could obtain the components representing turbulence accompanying the wave motion, giving room for estimating some of its traditional parameters. This decomposition and subsequent analysis proved successful both for the lake and the lagoon, for Lake Neusield even offering to evaluate their depth-dependence.

In Lake Neusiedl rather low turbulent kinetic energy level and the presence of short time period energetic turbulent eddies were found at low wind speed, significantly elevated with increasing wind. The estimated Eulerian timescale showed isotropy in the vertical plane of the wave motion whereas anisotropy perpendicular to that. Synchronised flow measurements at two depths have shown their merits, encouraging using even more sensors simultaneously, based on which wind-induced analytical profiles with more than two parameters could be reconstructed. Moreover, the measurement and estimation of the main wave and turbulence parameters should be extended also to the reed zone, where the exploration of their attenuation tendency could improve the description of the siltation processes in the littoral-pelagic interface region.

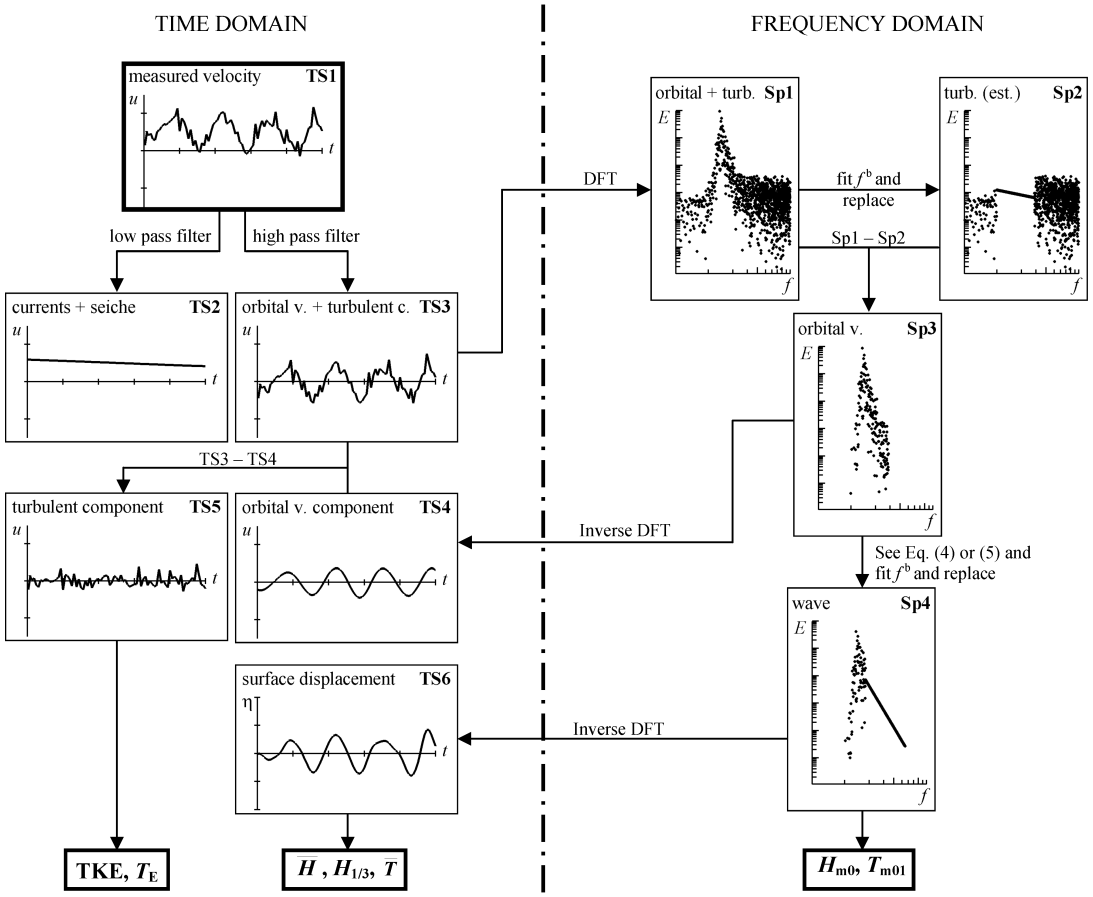

Fig. 24. The flowchart describing the reconstruction of the wave and turbulence features from 3D velocity time series.

References

1 **Baranya S, Józsa J**, *Flow Analysis in River Danube by Field Measurement and 3D CFD turbulence modelling*, Periodica Polytechnica, Civil Enginnering, **50**(1), (2006), 57–68.

2 **Bricker J D, Monismith S G**, *Spectral wave-turbulence decomposition*, Journal of Atmospheric and Oceanic Technology, **24**(8), (2007), 1479–1487.

3 **Dean R G, Dalrymple R A**, *Water wave mechanics for engineers and scientists*, Prentice-Hall, 1984.

4 **Massel S R**, *Ocean surface waves: their physics and prediction*, Word Scientific, 1996.

5 **Krámer T, Józsa J**, *An adaptively refined, finite-volume model of wind-induced currents in Lake Neusiedl*, Periodica Polytechnica, Civil Enginnering, **49**(2), (2005), 111–136.

6 **Prevosto M, Krogstad H E, Barstow S F, Soares C G**, *Observations of the high-frequency range of the wave spectrum*, Journal of Offshore Mechanics and Arctic Engineering, **118**(2), (1996), 89–95.

7 **Rodríguez G, Soares C**, *Uncertainty in the estimation of the slope of the high frequency tail of wave spectra*, Journal of Applied Ocean Research, **21**(4), (1999), 207–213.

8 *Guide to wave analysis and forecasting*, World Meteorological Organization, Geneva, Switzerland, 1998.